Reflective Characteristics of Spatially-Bounded Laser Beam by Rugate coating

Zheng Guangwei

Information and Navigation College, Air Force Engineering University, 710077, Xi'an, Shannxi, China

Email: zgw198196@126.com

Abstract. Based on the transfer matrix analysis and discrete Fourier transform, the reflective characteristics of a spatially-bounded laser beam by a Rugate coating are investigated. The spatial intensity distribution and reflectance efficiency of the reflected beam are formulated. When the central vector of the laser beam satisfies the coating's Bragg law, the spatial intensity distributions of the diffracted beam with the change of the coating's parameters are simulated. The results show that with the decrease of the thickness, the increase of the period, or the decrease of the relative permittivity modulation, the spatial intensity distributions of the reflected beam in the incidence plane are broadened compared with those of incident beam, while those perpendicular to the incidence plane are not. And the reflectance efficiencies decrease. Among these three parameters, the relative permittivity modulation and thickness influence the reflectance characteristics a lot, while the period influences the reflectance characteristics a little. It means that when the thickness decreases, or modulation decreases, the Rugate coating has finer angular selective characteristics and less angular selectivity bandwidth. The results are instructive for the design and application of Rugate coating.

1. Introduction

Rugate coating is a type of thin films, the refractive index of which changes continuously along its thickness[1]. Compared with the traditional graded coatings, Rugate coating has many merits, such as no harmonious reflective bands, low stress between different layers, high laser damage threshold, and so on[2, 3]. The characteristics of Rugate coatings have been analyzed since 1960s[4]. However, with the development of modern coating's technique, Rugate coating's application has attracted lots of attention recently[5-7].

Spatial filter can improve the laser beam quality in the spatial domain, which is very important for its usage, such as the ignition laser beams in the Inertial Confinement Fusion system, and so on[8-9]. Nowadays, the most widely-used spatial filter is pinhole filter, the structure of which is two lens aligned coaxially with a pinhole plate placed in the con-focusing plane in order to select the required angular spectrum. Due to its focusing characteristics, pinhole filter cannot be adjusted easily to the application for the high power laser beam because of the higher beam intensity around the pinhole[10-12]. So the non-focusing methods have attracted a lot of attention. Due to the fine wave vector selectivity of the coatings, the non-spatial filtering for laser beam based on coatings has been put forward since 2000s[13,14]. The fine wave vector selectivity denotes the fine wavelength selectivity at some angular domain and the fine angular selectivity at some wavelength domain. So Rugate coatings may be a potential candidate for the pinhole filter, especially in the high power laser field, with its fine angular selectivity[15]. However, there

is lots of attention paid to the reflectance or transmittance characteristics of the Rugate coating for the wavelength spectrum or angular spectrum, while there is little attention paid to the reflectance characteristics of the Rugate coating for the actual laser beam. Maybe the reflected laser beam is spatially deformed compared with the incident spatially-bounded laser beam by the Rugate coating. So it is necessary to calculate the reflectance characteristics of the Rugate coating for the real laser beam.

2. Configuration and Theoretical Analyses

Fig.1 shows the spatially-bounded laser beam incident into a Rugate coating.

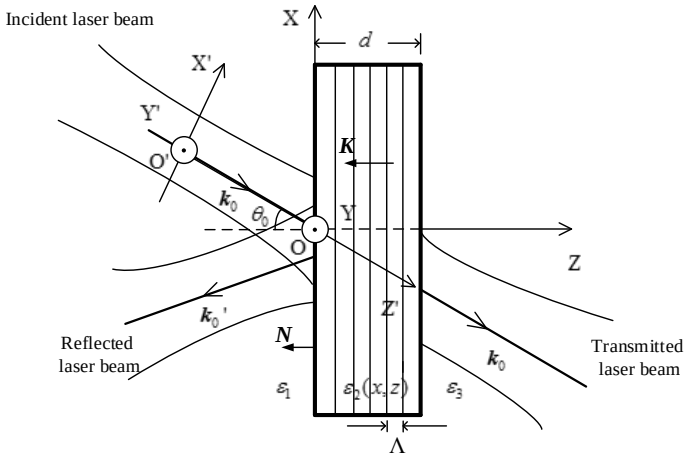

Fig.1. Schematic of spatially-bounded laser beam incident into a Rugate coating

In fig.1, the solid parallel lines stand for the coating's fringes. Λ denotes the period, d denotes the thickness. **K** denotes the coating's vector. Without any loss of generality, **K** is selected to be in the XOZ plane. $\varepsilon_2(\mathbf{r})$ is the coating's relative permittivity, which can be expressed as:

$$\varepsilon_2(\mathbf{r}) = \varepsilon_{20} + \varepsilon_{21}\cos(\mathbf{K}\cdot\mathbf{r}) \tag{1}$$

where ε_{20} and ε_{21} denote the relative mean dielectric permittivity and its modulation amplitude, respectively. **r** denotes the position vector, stands for (x, y, z). X' axis is in the plane of incidence, which is formed by the central wave vector $\mathbf{k}_0$ of the incident laser and the coating's front surface normal **N**, while Y' axis is orthogonal to the plane of incidence. And Z' axis is parallel to $\mathbf{k}_0$. θ_0 is the incidence angle between $\mathbf{k}_0$ and Z axis. ε_1 and ε_3 are the relative permittivities in region 1 and region 3, respectively.

2.1. Decomposition of the spatially-bounded laser beam by discrete Fourier transforms

Based on the deduced reflectance results of a Rugate coating illuminated by monochromatic plane waves (MPWs) based on the transfer matrix analysis (TMA)[16,17], intuitively the spatially-bounded laser beam should be firstly transformed into linear combinations of MPWs based on the two-dimensional discrete Fourier transforms in spatial domains. And secondly the reflected and transmitted characteristics of each MPW can be achieved depending on the TMA. Finally based on the inverse discrete Fourier transform, the spatial intensity distributions of reflected laser beam can be formulated.

The field amplitude of incident laser beam (at $Z=0$) can be expanded into linear combinations of MPWs as:

$$E_v\left(x_{n_1}, y_{n_2}, z=0\right) = \sum_{m_1=-M_1/2}^{M_1/2-1}\sum_{m_2=-M_2/2}^{M_2/2-1} F_v\left(k_{x,m_1}, k_{y,m_2}, z=0\right)\exp\left[-j\left(k_{x,m_1}x_{n_1} + k_{y,m_2}y_{n_2} + k_{z,m_1,m_2,p}z\right)\right] \tag{2}$$

where M_1 and M_2 are the numbers of sampling points over the spatial intervals $-D_1/2 \le x_{n_1} \le D_1/2$, and $-D_2/2 \le y_{n_2} \le D_2/2$, in X and Y axis respectively. $k_{x,m_1} = m_1(2\pi/D_1)$ and $k_{y,m_2} = m_2(2\pi/D_2)$

are the wave vector components along X and Y axis, respectively. Furthermore, the z wave vector component for MPW (m_1, m_2) can be achieved by $k_{z,m_1,m_2} = \left(k_0^2\varepsilon_1 - k_{x,m_1}^2 - k_{y,m_2}^2\right)^{1/2}$. $k_0 = \omega_0/c$, c denotes the light speed in vacuum. Subscript v stands for x, y, or z, which means the polarization in the X, Y, or Z axis.

Furthermore, the corresponding monochromatic plane-wave spectrum coefficient for MPW (m_1, m_2) can be performed by

$$F_v\left(k_{x,m_1}, k_{y,m_2}, z=0\right) = \frac{1}{M_1 M_2} \sum_{n_1=-M_1/2}^{M_1/2-1} \sum_{n_2=-M_2/2}^{M_2/2-1} E_v\left(x_{n_1}, y_{n_2}, z=0\right) \times \exp\left[j\left(k_{x,m_1} x_{n_1} + k_{y,m_2} y_{n_2} + k_{z,m_1,m_2} z\right)\right] \tag{3}$$

where $\mathrm{x}_{n_1} = n_1 D_1 / M_1$, $\mathrm{y}_{n_2} = n_2 D_2 / M_2$.

For MPW (m_1, m_2), the incidence angle θ_{m_1,m_2} can be performed by

$$\theta_{m_1,m_2} = \cos^{-1}\left[k_{z,m_1,m_2} \Big/ \left(k_0 \varepsilon_1^{1/2}\right)\right] \tag{4}$$

2.2 Intensity distributions of the reflected laser beam in spatial domains

Assuming the incident laser beam is TE mode, and based on the deduced conclusions of TMA, the reflected amplitude of each MPW (m_1, m_2) can be determined by

$$F_{yD}^R\left(k_{x,m_1}', k_{y,m_2}', 0\right) = E_R(\lambda_0, \theta) F_y\left(k_{x,m_1}, k_{y,m_2}, 0\right) \tag{5}$$

where $\lambda_0 = 2\pi/k_0$, $k_{x,m_1}' = k_{x,m_1}$, $k_{y,m_2}' = k_{y,m_2}$, $E_R(\lambda_0, \theta)$ denotes the reflected coefficient for each MPW based on TMA.

As a result, the amplitude of the reflected laser beam is expressed as:

$$\begin{aligned} E_{yD}^R\left(x_{n_1}, y_{n_2}, z\right) = & \sum_{m_1=-M_1/2}^{M_1/2-1} \sum_{m_2=-M_2/2}^{M_2/2-1} F_{yD}^R\left(k_{x,m_1}', k_{y,m_2}', 0\right) \\ & \times \exp\left[-j\left(k_{x,m_1}' x_{n_1} + k_{y,m_2}' y_{n_2} + k_{z,m_1,m_2}^R{}' z\right)\right] \end{aligned} \tag{6}$$

where $k_{z,m_1,m_2}^R{}'$ denotes the projection of $\boldsymbol{k}_{m_1,m_2}^R{}'$ into Z axis. And it can be expressed as:

$$k_{z,m_1,m_2}^R{}' = \begin{cases} -\left(k_0^2\varepsilon_1 - k_{x,m_1}^2{}' - k_{y,m_2}^2{}'\right)^{1/2} & k_{x,m_1}^2{}' + k_{y,m_2}^2{}' \le k_p^2\varepsilon_3 \quad \textit{transmitting waves} \\ +j\left(k_{x,m_1}^2{}' + k_{y,m_2}^2{}' - k_0^2\varepsilon_3\right)^{1/2} & k_{x,m_1}^2{}' + k_{y,m_2}^2{}' > k_p^2\varepsilon_3 \quad \textit{evanescent waves} \end{cases} \tag{7}$$

So the intensity distribution of the reflected laser beam can be expressed as:

$$\begin{aligned} I_{sD}^R\left(x_{n_1}, y_{n_2}, z\right) = & \left| \sum_{m_1=-M_1/2}^{M_1/2-1} \sum_{m_2=-M_2/2}^{M_2/2-1} F_{yD}^R\left(k_{x,m_1}', k_{y,m_2}', 0\right) \right. \\ & \left. \times \exp\left[-j\left(k_{x,m_1}' x_{n_1} + k_{y,m_2}' y_{n_2} + k_{z,m_1,m_2}^R{}' z\right)\right] \right|^2 \end{aligned} \tag{8}$$

And the reflectance efficiency is:

$$\eta_D^R = \frac{\sum_{m_1=-M_1/2}^{M_1/2-1} \sum_{m_2=-M_2/2}^{M_2/2-1} \left| F_{yD}^R\left(k_{x,m_1}', k_{y,m_2}', 0\right)\right|^2}{\sum_{m_1=-M_1/2}^{M_1/2-1} \sum_{m_2=-M_2/2}^{M_2/2-1} \left| F_y\left(k_{x,m_1}, k_{y,m_2}, 0\right)\right|^2} \tag{9}$$

3. Simulation results

The Gaussian laser beam has been widely used in lots of optical systems, so we select Gaussian laser beam as the incident spatially-bounded laser beam. For simplicity, the dispersion is not considered in the paper. The laser's normalized amplitude is expressed as

$$\mathbf{E}(x',y',z',t)=\frac{w_0}{w(z')}exp\left[-\left(x'^2+y'^2\right)/w^2(z')\right] \times exp\left\{j\left[(\omega_0 t-\mathrm{k}_0\cdot z')-k_0\frac{\left(x'^2+y'^2\right)}{2R(z')}-\tan^{-1}\left(\frac{z'\lambda_0}{\pi w_0^2}\right)\right]\right\}\cdot \boldsymbol{y} \tag{10}$$

where w_0 is the beam waist radius. $\boldsymbol{y}$ is the unit vector along y axis.

$$w(z')=w_0\left\{1+\left[z'\lambda_0/\left(\pi\omega_0^2\right)\right]^2\right\}^{1/2} \tag{11}$$

$$R(z')=z'+\left(\pi\omega_0^2/\lambda_0\right)^2/z' \tag{12}$$

where $w(z')$ and $R(z')$ are the beam radius and the phase front curvature radius at the distance z' away from the beam waist center, respectively.

In the practical application, the highest diffraction efficiency is the key factor for the Rugate coating. So we just consider the condition that the central wave vector of the incident laser pulse satisfies the coating's Bragg's law, which is a requisite condition for its greatest reflectance efficiency of this kind of laser beam. And it can be expressed as:

$$2|\boldsymbol{k}_0|\varepsilon_{20}\cos\theta_0=|\boldsymbol{K}| \tag{13}$$

The other parameters used in the simulation are shown in tab.1.

Tab.1. Parameters and quantities in the simulation

Parameter	Quantity	Parameter	Quantity
λ_0	1053 nm	ε_1, ε_3	2.250
D_1, D_2	310 μm	M_1, M_2	310
w_0	50 μm	ε_{20},	2.250

3.1 Spatial intensity distributions of the reflected beam with the change of the relative dielectric permittivity modulation

Three groups of parameters are selected, with the relative dielectric permittivity modulation of 0.01 ppm, 0.02 ppm, or 0.03 ppm, respectively. The coating's thickness is 100 μm. The grating's period is 380 nm. The spatial intensity distributions of the reflected laser with the change of the relative permittivity modulation is shown in figure 2.

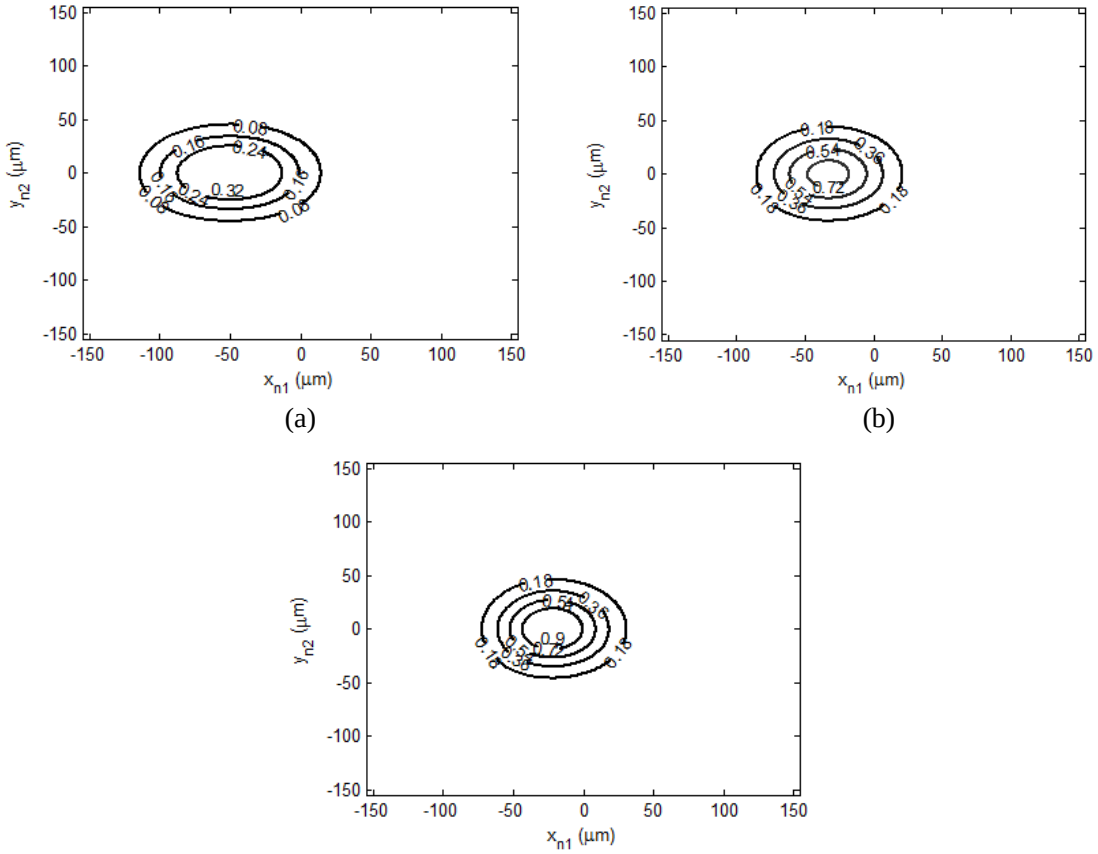

Fig.2. Spatial intensity distributions of reflected laser beam with the coating's relative permittivity modulation of (a) 0.01, (b) 0.02, and (c) 0.03.

From figure 2, we can deduce that with the relative permittivity modulation's increment, the intensity distributions of the reflected laser are getting more and more similar to that of the input laser in the spatial domain. It means that more decomposed MPWs are reflected at the higher relative dielectric permittivity modulation than those at the lower one. And when the relative dielectric permittivity modulation is low, the profile in X axis is widened greatly, which means some higher angular frequencies are not reflected. It is shown that the spatial width in the Y axis is approximately the same as that of the input one, which means that the Rugate coating has little effect on the wave vector components that are perpendicular to incidence plane. The reflectance efficiencies are 52.36%, 91.26%, and 98.96% in correspondence to the relative permittivity modulation of (a) 0.01, (b) 0.02, and (c) 0.03, respectively.

3.2 Spatial intensity distributions of the reflected beam with the change of the coating's thickness

In this part, three groups of coating's parameters are selected, with the coating's thickness of 50μm, 100μm, or 150μm, respectively. The relative dielectric permittivity modulations are fixed as 0.02. The grating's periods are 380nm. The spatial intensity distributions of the reflected laser with different gratings' thickness are shown in figure 3.

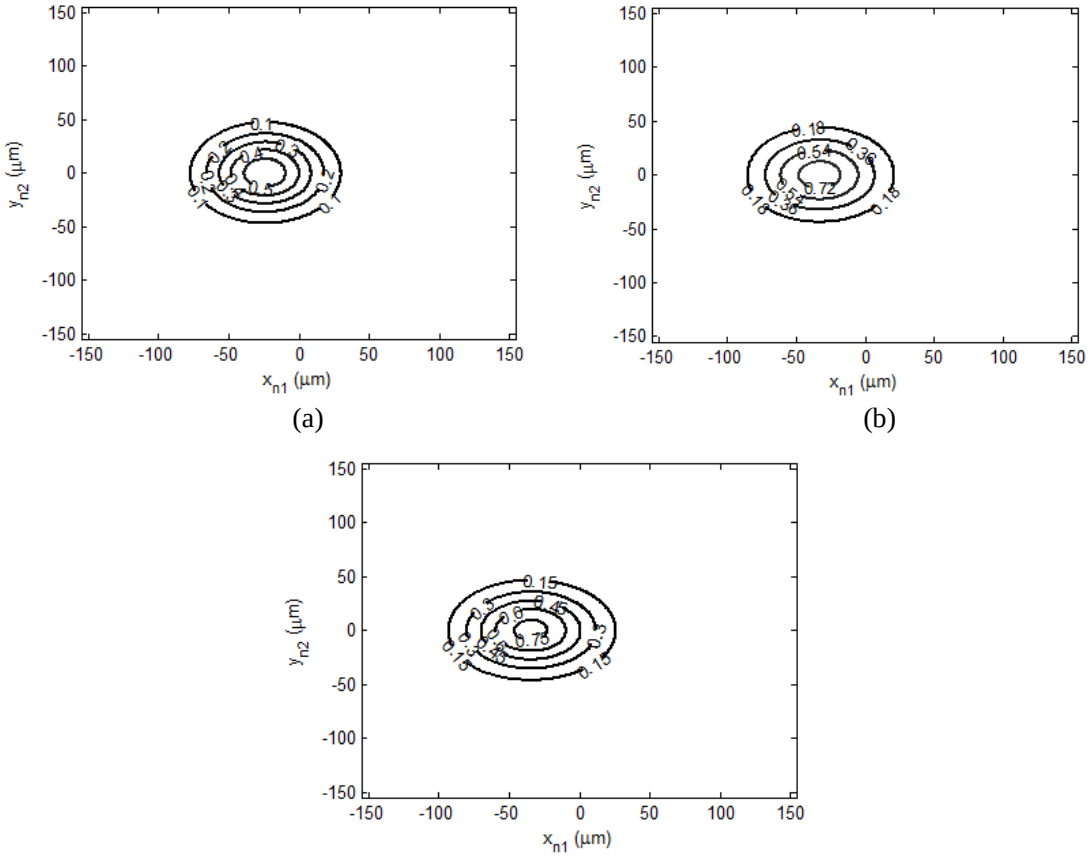

Fig.3. Spatial intensity distributions of reflected laser beam with the coating's thickness (a) $d = 50\mu m$; (b) $d = 100\mu m$; (c) $d = 150\mu m$

From figure 3, we can deduce that with the thickness's increment, the intensity distributions of the reflected laser are similar to those of the input laser in the spatial domain firstly. And then it spreads along the X axis. It means that when the coating's thickness is small, the angular selectivity bandwidth is wide. Although at this situation, the diffraction efficiency is not high, most of the decomposed MPWs are reflected. With the thickness's increment, the diffraction efficiency gets higher. But due to the narrow angular selectivity bandwidth, the spatial intensity distribution of the reflected beam is broadened. The reflectance efficiencies are 60.18%, 91.26%, and 96.05% with respect to the thickness of 50μm, 100μm, and 150μm, respectively.

3.3 Spatial intensity distributions of the reflected beam with the change of the coating's periods

Three groups of coating's parameters are selected, with the coating's periods 360μm, 380μm, or 400μm, respectively. The relative dielectric permittivity modulations are fixed as 2500ppm. The grating's periods are 380nm. The spatial intensity distributions of the reflected laser with different gratings' thickness are shown in figure 4.

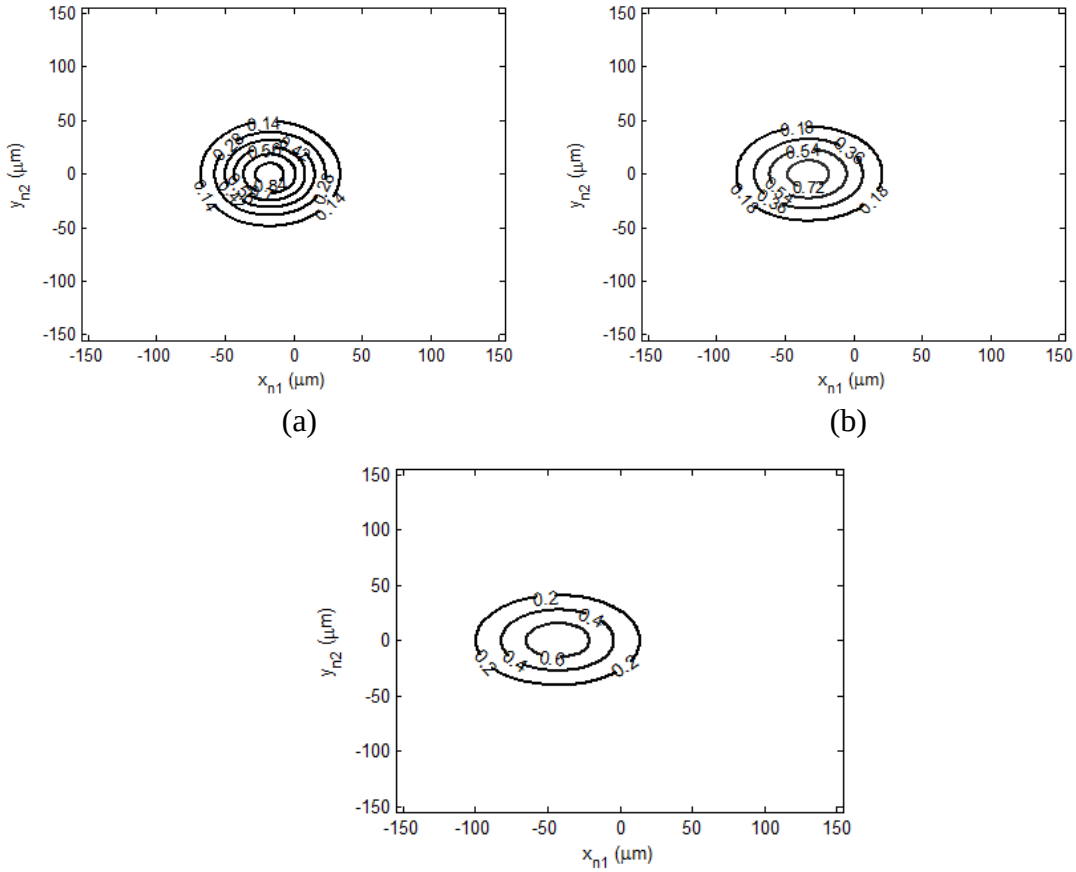

(a) (b)

(c)

Fig.4. Spatial intensity distributions of reflected laser beam with the coating's period
(a) $\Lambda = 360\mu m$; (b) $\Lambda = 380\mu m$; (c) $\Lambda = 400\mu m$

From figure 4, we can deduce that with the period's increment, the intensity distributions of the reflected laser are broadened in the X axis compared with that of the input laser in the spatial domain. It means that less decomposed MPWs are reflected at the higher period than those at the smaller one. So the angular selectivity bandwidth is thinner with the higher period. The reflectance efficiencies are 89.46%, 91.26%, and 92.58% with respect to the period of 50μm, 100μm, and 150μm, respectively. It means that the period's change does not influence the diffraction efficiency very much.

4. Conclusions

We analyze the reflective characteristics of a Rugate coating illuminated by a spatially-bounded laser beam. Besides the reflectance efficiency, the spatial intensity distribution is put forward with the change of the different coating's parameter. The results show that with the decreasing of the grating's period, increasing of its thickness, and increasing of its relative dielectric permittivity modulation, the spatial intensity distribution of the reflected laser are similar to those of the input pulse. dAnd the reflectance efficiencies increase. Among these three parameters, the relative permittivity modulation and thickness influence the reflectance characteristics a lot, while the period influences the reflectance characteristics a little. It means that when the thickness decreases, or modulation decreases, the Rugate coating has finer angular selective characteristics and less angular selectivity bandwidth. The results are instructive for the design and application of Rugate coating.

Acknowledgement
The author acknowledges the support of National Natural Science Foundation of China (No.61205002).

References

[1] Bertrand G. Bovard 1993 Rugate filter theory: an overview *Appl. Opt* **32** 5427
[2] W. H. Southwell 1988 Spectral response calculations of rugate filters using coupled-wave theory *Appl. Opt* **28** 2949
[3] T. Herffurth et al 2014 Roughness and optical losses of rugate coatings *Appl. Opt* **53** A351
[4] Erwin Delano 1967 Fourier synthesis of multilayer filters *JOSA* **57** 1529
[5] Andy C. van Popta et al 2004 Gradient-index narrow-bandpass filter fabricated with glancing-angle deposition *Optics Letters* **29** 2545
[6] Xinbin Cheng et al 2008 Gradient-index optical filter synthesis with controllable and predictable refractive index profiles *Optics Express* **16** 2315
[7] P. V. Usik et al 2009 Spatial and spatial-frequency filtering using one-dimensional graded-index lattices with defects *Optics Communications* **282** 4490
[8] J. T. Hunt et al 1978 Suppression of self-focusing through low-pass spatial filtering and relay imaging *Appl. Opt* **17** 2053
[9] Liu Daizhong et al 2006 Design and application of a laser beam alignment system based on the imaging properties of a multi-pass amplifier *Chinese optics letters* **4** 601
[10] Liu Daizhong et al 2006 Design and application of a laser beam alignment system based on the imaging properties of a multi-pass amplifier *Chinese optics letters* **4** 601
[11] A. K. Potemkin et al 2007 Spatial filters for high-peak-power multistage laser amplifiers *Appl. Opt* **46** 4423
[12] Bonghoon Kang et al 2010 Optimization of the input fundamental beam by using a spatial filter consisting of two apertures *Journal of the Korean Physical Society* **56** 325
[13] Ivan Moreno and J. Jesus Araiza 2004 Thin-film optical filters for spatial frequencys *Proc. of SPIE* **5524** 409
[14] Ivan Moreno et al 2005 Thin-film spatial filters *Optics Letters* **30** 914
[15] Luo Zhaoming et al 2010 Low-pass rugate spatial filters for beam smoothing *Optics communications* **283** 2665
[16] M. G. Moharam and T. K. Gaylord 1982 Chain-matrix analysis of arbitrary-thickness dielectric reflection gratings *JOSA* **72** 187
[17] David J. Mccartney 1989 The analysis of volume reflection gratings using optical thin-film techniques *Optical and quantum electronics* **21** 93